JOURNAL OF GEOPHYSICAL RESEARCH, VOL. 89, NO. B12, PAGES 10,341–10,354, NOVEMBER 10, 1984

Transitional Paleointensities From Kauai, Hawaii, and Geomagnetic Reversal Models

SCOTT W. BOGUE[1]

U.S. Geological Survey, Menlo Park, California

ROBERT S. COE

Earth Sciences Board, University of California, Santa Cruz

Thellier paleointensity results from an R-N transition zone in Kauai, Hawaii, show that field intensity dropped from 0.431 Oe to 0.101 Oe while the field remained within 30° of the reversed axial dipole direction. A recovery in intensity and the main directional change followed this presumably short period of low field strength. As the reversal neared completion, the field had an intensity of 0.217 Oe while still 40° from the final direction. The relationship of paleointensity to field direction during the early part of the reversal thus differs from that toward the end, a feature that only some reversal models are consistent with. For example, a model in which a standing nondipole component persists through the dipole reversal predicts only symmetric intensity patterns. In contrast, zonal flooding models generate suitably complex field behavior if multiple flooding schemes operate during a single reversal or if the flooding process is itself asymmetric.

INTRODUCTION

Paleomagnetic evidence demonstrates conclusively that the earth's field has reversed frequently in the geologic past, but our knowledge of the duration, configuration and, in particular, the intensity of the transitional field remains very limited. Most geologic environments are not able to record intermediate fields with much detail simply because reversals proceed at a geologically rapid pace. The problem of transitional field intensities is even more troublesome. Only a few of the available reversal records are amenable to paleointensity techniques and, consequently, many fundamental questions remain unanswered: Does field intensity vary in a systematic way during field reversals? How low or high can transitional fields get? What is the relative timing of changes in intensity and direction during reversals?

Current ideas on the intensity of transitional fields are based on a very small set of reliable data. The lowest absolute paleointensities reported from volcanic reversal records are 0.11 Oe (*Coe* [1967*a*], using the method of *Thellier and Thellier* [1959]) and 0.02 Oe (*Shaw* [1975], using the method of *Shaw* [1974]. These results substantiate the general inference, based on the low natural remanent magnetization (NRM) intensities in most transition zones, that the field intensity diminishes greatly during reversals. For the R3-N3 reversal in Iceland, *Shaw* [1975] found that the ancient field intensity became low just before the major change in direction. This behavior is consistent with what *Opdyke et al.* [1973] observed in marine sediments but contrasts with the longer interval of lowered NRM intensity in the sediments of Lake Tecopa [*Hillhouse and Cox*, 1976] and in the Tatoosh intrusion [*Dunn et al.*, 1971; *Dodson et al.*, 1978]. Such inferences from sedimentary and intrusive rocks all depend on the questionable assumption that variations in the ancient field intensity are accurately reflected in the NRM pattern. Taken at face value, however, the evidence implies that the behavior of transitional field intensity may vary substantially from place to place or from reversal to reversal. Finally, *Shaw*'s [1975] results from the R3-N3 reversal suggest that the transitional field intensity may sometimes reach high values. Whether such behavior is really a characteristic of some reversals and whether the field may also become unusually strong immediately before or after reversals [*Van Zijl et al.*, 1962; *Dunn et al.*, 1971; *Kaporovich et al.*, 1966] require further confirmation by careful paleointensity studies.

In this paper, we add to the small set of data from volcanic rocks with paleointensity results from a reverse to normal (R-N) transition zone of Pliocene age from Kauai, Hawaii. The paleomagnetic directions from this transition zone, as well as those from the succeeding N-R zone, previously appeared to be consistent with either of two simple reversal models [*Bogue and Coe*, 1982]. However, neither of the models in their simplest form can explain the intensity results from the R-N reversal record.

TRANSITION ZONES ON KAUAI

Paleomagnetic Directions: R-N

Paleomagnetic surveys of the Hawaiian Islands in the late sixties and early seventies [e.g., *Tarling*, 1965; *Doell and Dalrymple*, 1973] revealed the presence of normally and reversely magnetized lavas but no depositional contacts between two polarities. Nevertheless, the pioneering work of *Doell* [1972] suggested the possibility of transition zones on Kauai; he found normal paleomagnetic directions at high elevations, and reversed directions lower, in Kauai's main basaltic shield. Guided by Doell's results, it was relatively straightforward for us to locate the R-N transition zone between the two. Further reconnaissance led to the discovery of the underlying N-R transition zone (which we have not examined in detail) as well as a second N-R boundary that directly succeeds the R-N horizon.

The R-N transition zone (informally referred to here as the Napali transition zone) occurs in the predominantly olivine basalt flows of the Napali Formation [*Macdonald et al.*,

[1] Now at Department of Geological Sciences, University of Washington, Seattle.

Paper number 4B0806.

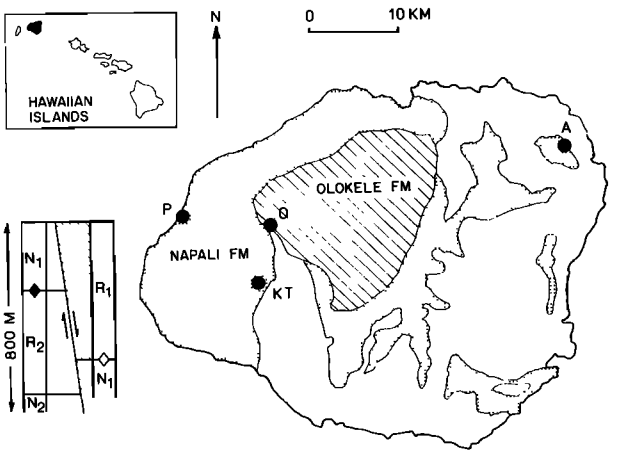

Fig. 1. Map showing outcrop extent of Napali and Olokele Formations and paleomagnetic sampling sites: P represents Polihale, KT represents Kukui Trail, O represents Kahililoa (in Olokele Formation), and A represents Anahola. Composite magnetostratigraphic columns show exposed thicknesses and relative positions of polarity units near the western caldera boundary. The youngest unit (R_1) is seen only in the Olokele Formation and the oldest (N_2) only in the Napali Formation (The polarity unit names are informal and apply only locally.) We show the sense of offset on the caldera boundary fault, but this offset may predate eruption of some Olokele flows. Closed (open) diamond shows the R-N (N-R) transition zone studied in detail.

1960]. The Napali flows, which constitute Kauai's main volcanic shield, are typically a few meters thick and dip away from the island's central region at angles from 6° to 12°. *McDougall* [1979] reports K-Ar ages of 3.8 to 5.1 m.y. from Napali basalts. We performed detailed sampling through the R-N transition at three localities (see Figure 1): in the sea cliffs at Polihale near the western extreme of the island, at a spot about one-half way down the Kukui Trail on the western wall of Waimea canyon, and on an erosional remnant of Napali flows near Anahola in the northeastern corner of the island. Additional details on the individual sites are given in Appendix A.

The laboratory procedure for determining the ancient field direction recorded by each flow was straightforward. Stepwise demagnetization experiments on a few samples from each flow demonstrated that secondary components of magnetization, if significant at all, could be greatly reduced by alternating field (AF) strengths of a few hundred Oersteds or less. In only one case (flow A5 from Anahola) was there a sample whose direction was unexplainably anomalous and far enough from the remaining samples to substantially affect the flow-mean direction. For this flow we report a mean direction both with and without the anomalous sample.

The directional data are listed in stratigraphic order in Tables 1–3 and plotted on equal area projections in Figure 2. These plots also show an expected direction of $D = 001°$,

TABLE 1. Kukui Trail (Napali Formation) Directional Results

Flow	Samples	Oe	N	α_{95}	k	D	I	Latitude	Longitude
KT32	8Q183–189	100	6	1.3	2509	359.5	32.0	88.3	041.1
KT31	8Q190–196	100	7	1.4	1823	359.8	32.7	88.8	034.0
KT30	8Q197–203	100	7	1.0	3839	002.1	33.3	87.8	317.0
KT29	8Q204–210	50	6	1.2	2904	013.4	27.2	76.4	312.7
KT28	8Q211–217	100	7	2.0	896	013.4	22.4	75.1	322.7
KT27	8Q218–224	···*	···*	···*	···*	···*	···*	···*	···*
KT26	8Q225–231	200	7	3.2	364	192.3	−16.6	−74.1	154.7
KT25	8Q232–238	200	7	2.9	425	190.3	−17.7	−75.9	158.5
KT24	8Q239–245	200	7	2.0	949	191.8	−22.1	−76.4	146.8
KT23	8Q246–252	300	7	4.8	159	191.0	−20.4	−76.4	152.0
KT22	8Q253–259	400	7	5.2	137	186.7	−16.6	−77.6	172.4
KT21	8Q260–266	···†	···†	···†	···†	···†	···†	···†	···†
KT19	8Q274–280	200	6	3.7	329	187.6	−18.3	−77.9	166.5
KT18	8Q281–287	200	6	3.1	468	163.6	−29.8	−74.1	286.6
KT17	8Q288–294	200	7	1.2	2359	159.4	−31.3	−70.3	292.2
KT16	8Q295–301	300	6	1.5	2106	160.1	−33.1	−71.1	295.3
KT15	8Q302–308	100	7	2.7	487	005.4	42.4	82.5	246.2
KT14	8Q309–315	100	7	2.0	898	157.7	−27.7	−68.2	287.0
KT13	8Q316–322	100	7	1.2	2504	158.9	−30.0	−69.7	290.1
KT12	8Q323–329	100	7	1.2	2452	159.2	−30.4	−70.0	290.7
KT11	8Q330–336	100	7	1.6	1414	158.6	−30.8	−69.5	291.7
KT10	8Q337–343	200	6	2.3	863	158.7	−30.9	−69.6	291.8
KT9	8Q344–350	200	7	4.4	191	158.1	−27.7	−68.6	286.8
KT8	8Q351–357	200	7	2.0	881	156.0	−26.2	−66.4	285.9
KT7	8Q358–364	300	7	2.0	910	166.2	−41.6	−76.3	318.5
KT6	8Q365–371	100	7	1.6	1361	166.4	−40.4	−76.7	315.1
KT5	8Q372–378	100	7	1.1	3031	170.3	−40.3	−80.1	321.2
KT4	8Q379–385	100	7	3.9	235	170.7	−45.3	−78.4	339.1
KT3	8Q386–392	100	7	2.4	663	169.3	−49.7	−74.9	347.0
KT2	8Q393–399	100	7	1.9	968	172.5	−53.6	−73.5	002.7
KT1	8Q400–406	100	7	1.7	1225	174.3	−52.8	−74.8	006.6

KT20 was an out of place block; Oe is the level of AF demagnetization; N is the number of samples included in the flow mean; α_{95} is the angular interval of 95% confidence in the mean direction, k is the precision parameter describing sample dispersion [*Fisher*, 1953]; D and I are the eastward declination and downward inclination of the mean direction; latitude and longitude are north latitude and east longitude of the VGP equivalent to the mean direction (calculated for a site at 19°N, 205°E).

*Thermally remagnetized by overlying flow.

†Very weak, scattered NRM.

TABLE 2. Anahola (Napali Formation) Directional Results

Flow	Samples	Oe	N	α_{95}	k	D	I	Latitude	Longitude
A19	9Q220–226	···†	···†	···†	···†	···†	···†	···†	···†
A18	9Q213–219	400	6	2.5	701	355.7	57.0	71.0	194.5
A17	9Q206–212	400	7	12.0	26.1	022.4	56.4	63.4	247.9
A16	9Q199–205	300	7	3.8	253	047.5	64.7	42.5	248.4
A15	9Q191–198	···‡	···‡	···‡	···‡	···‡	···‡	···‡	···‡
A14	9Q184–190	100	7	2.8	455	157.1	10.0	−57.0	250.4
A13	9Q177–183	200	7	2.6	543	149.8	−08.8	−57.1	272.5
A12	9Q170–176	200	7	5.4	125	147.6	−03.7	−53.9	270.5
A11	9Q163–169	200	7	4.2	211	145.9	−08.1	−53.5	275.2
A10	9Q156–162	200	7	3.3	335	143.1	−13.9	−52.2	281.6
A9	9Q227–233	···†	···†	···†	···†	···†	···†	···†	···†
A8	9Q149–155	200	7	2.7	513	153.0	−18.7	−62.2	279.0
A7	9Q142–148	200	7	5.1	140	154.9	−16.5	−63.5	275.0
A6	9Q135–141	300	7	7.0	75.3	150.7	−10.0	−58.2	272.7
A5	9Q128–134	400	7	11.6	28.1	161.6	−22.7	−70.9	275.6
	(w/o 130)		6	2.6	690	155.7	−22.1	−65.4	280.7
A4	9Q121–127	200	7	8.6	50.7	150.6	−15.3	−59.3	277.6
A3*	9Q114–120	200	7	2.1	814	009.3	62.1	64.4	220.8
A2	9Q107–113	50	7	2.4	631	174.2	−26.9	−82.7	255.2
A1	9Q100–106	100	7	1.9	983	178.5	−27.0	−85.1	222.2

For explanation, see Table 1.
*A sill with a direction similar to flows higher in the section.
†Lightning.
‡Thermally remagnetized by overlying flow.

$I = 35°$ for comparison. This direction is the axial dipole direction appropriate for a rock magnetized 5 m.y. ago at the present latitude (19°N) of the big island of Hawaii (Pacific plate reference pole of *Turner et al.* [1980]). At the base of the Kukui Trail section, the reversely magnetized flows have declinations close to 170° and negative inclinations slightly steeper than expected. Moving up section, the directions shallow and become more easterly. A single flow (KT15) with a typical normal field direction occurs among these lower flows. The southeasterly directions are followed by directions that are also shallow but more southerly, and flows with normal directions immediately overlie those.

The anomalous direction in flow KT15 deserves special mention. We carefully examined this unit in the field and are convinced that it is a flow and not a sill. Examples of the latter, which are fairly common on Kauai, are easily recognized by their distinctive jointing and much greater resistance to weathering. Paleointensity work on flow KT15 was not possible because of minor low-temperature oxidation (apparent in strong-field thermomagnetic experiments), but the remanence was well-behaved. Only a single component was present, and NRM intensity, between-sample scatter, and AF stability were typical of Napali basalt flows. The normal-like direction preserved in the flow implies that the transitional field at Kauai moved, possibly rapidly, from a near-reversed to a near-normal direction and back again. Similar behavior has been observed in other reversal records such as those from Steens Mountain [*Watkins*, 1969] and the Tatoosh intrusion [*Dunn et al.*, 1971; *Dodson et al.*, 1978].

We sampled 18 flows and a sill at Anahola; the relevant data are in Table 2. For three flows, A9, A19, and A15, the NRM directions were very scattered. Overprints due to lightning (in the first two cases) and thermal remagnetization by the overlying flow (in the latter case) could not be removed by AF demagnetization. Directions from the other flows at Anahola show a trend similar to that seen in flows from the Kukui Trail site (see Figure 2), one difference being that the southeasterly directions shallow further than at the Kukui Trail and finally move through the horizontal plane.

The directions from 13 flows at Polihale are listed in Table

TABLE 3. Polihale (Napali Formation) Directional Results

Flow	Samples	Oe	N	α_{95}	k	D	I	Latitude	Longitude
P13	9Q001–007	100	7	1.6	1351	000.8	48.5	79.5	208.8
P12	9Q008–015	100	8	1.4	1531	355.0	46.3	80.2	177.9
P11	9Q016–021	100	3	4.9	624	357.2	25.3	83.7	050.7
P10	9Q022–030	100	9	1.4	1300	014.3	34.0	76.5	294.2
P9	9Q031–037	300	7	2.5	603	161.6	−46.5	−71.0	325.9
P8	9Q038–045	100	8	3.9	203	159.9	−44.2	−70.2	319.1
P7	9Q046–052	300	7	3.5	294	163.6	−46.3	−72.7	327.9
P6	9Q053–059	125	7	4.3	202	168.6	−51.8	−73.1	349.9
P5	9Q060–069	200	10	1.2	1704	170.1	−51.9	−73.8	353.6
P4	9Q070–075	100	6	3.1	468	173.7	−50.2	−76.7	000.8
P3	9Q076–081	100	6	1.5	2054	170.1	−47.3	−76.9	343.1
P2	9Q082–088	100	7	2.1	841	172.8	−47.2	−78.6	351.2
P1	9Q089–095	100	7	4.1	218	184.1	−50.7	−77.0	040.8

For explanation, see Table 1.

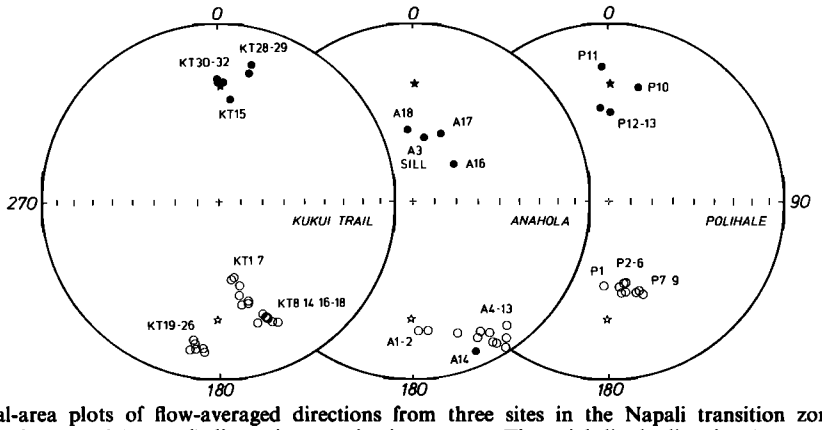

Fig. 2. Equal-area plots of flow-averaged directions from three sites in the Napali transition zone. Solid (open) symbols indicate downward (upward) directed magnetization vectors. The axial dipole direction (represented by stars) is shown for comparison.

3 and plotted in Figure 2. Flows with normal directions directly overlie those with reversed directions; no transitional field directions were recorded.

To get the fullest possible picture of how the field behaved during the R-N transition, it is necessary to combine the results from the three sites. This introduces a degree of uncertainty because there are several ways such a correlation could be made. There is little question, however, that the three sections record the same field reversal. In extensive surveys using a portable fluxgate magnetometer, all Napali flows that we examined above the R-N transition were normally magnetized, whereas all those in the first 450 m below were reversed; there was no evidence of short polarity intervals. This simple magnetostratigraphy suggests that volcanism during the early, shield-building stage of the island's growth was both continuous and rapid. Others [*Macdonald*, 1960; *Jackson et al.*, 1971; *McDougall*, 1979] have reached a similar conclusion on the basis of geological and geochronological evidence.

In addition, the elevation of the reversal horizon decreases smoothly with distance from the central caldera. Near the caldera boundary, the R-N horizon occurs at 951 m (3120 ft), whereas at the coast, approximately 8 km away, the horizon occurs at 183 m (600 ft). Without exception, reversal sites at distances intermediate between these two lie near a surface that slopes 5°, on the average, away from the island's center. This figure is comparable to the dips typical of Napali flows and thus is consistent with the other evidence that the R-N sites all belong to the same reversal horizon.

Finally, the similarity of paleomagnetic directions at the Kukui Trail and Anahola sites supports the idea that both have recorded the same reversal. The most likely correlation of directions between the sites is based on the trend of the shallow, southeasterly directions seen at the Kukui Trail and Anahola sites. At the former site, the field shallows and moves toward the east from $D = 174.3°$, $I = -52.8°$ (flow KT1) to $D = 163.6°$, $I = -29.8°$ (flow KT18). At Anahola, flow A5 has a direction that is further east and shallower still; D = 155.7°, I = −22.1°. In subsequent flows at Anahola, the direction shallows by another 32° to $D = 157.1°$, $I = 10.0°$ (flow A14). The trend from KT1 to A14 is thus continuous and clearly defined and is the key to the correlation of the flows between the two sites.

The next directions to occur in the Kukui Trail sequence are shallow and southerly. At Anahola, steep northwesterly directions follow. Therefore, unless the field first turned northerly and then resumed its reversed orientation, it is simplest to follow the sequence KT1-A14 with the shallowly magnetized flows KT19-KT26 and then by steep northerly flows A16-A18. This sequence encompasses the middle portion of the reversal record. The low reversed flows at Anahola, the normal and reversed flows from Polihale and high normal flows at the Kukui Trail can be added to the ends of the sequence in a straightforward fashion. The following composite sequence is the simplest way to correlate the three sections (stratigraphically lowest flows first): A1-A2, P1-P4, KT1-KT2, P5-P9 and KT3, KT4-KT18, A4-A14, KT19-KT26, A16-A18, P10, KT28-KT29, P11, KT30-KT32, and P12-P13. We used this sequence to construct the plot in the left-hand side of Figure 3.

In summary, the Napali flows show the field reversing by rotating downward from the reversed direction. A temporary and perhaps rapid flip to a normal-like direction occurred while the field was still close to its reversed direction. At some point between flow KT26 and A16, it appears likely that the field direction was almost vertical (downward). The equivalent VGP path must have passed close to Kauai and thus, using *Hoffman*'s [1977] terminology, was "near-sided." It is impor-

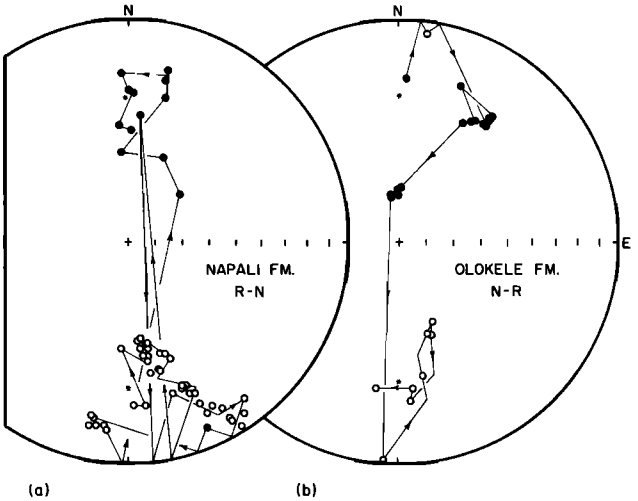

Fig. 3. (*a*) Equal-area plot of flow-averaged directions from the R-N transition zone. Results from the three sites in the Napali Formation are combined. Solid (open) symbols indicate downward (upward) directed magnetization vectors. The axial dipole direction (asterisk) is shown for comparison. (*b*) Directions from the N-R transition zone in the Olokele Formation.

tant to notice that this basic observation is independent of any particular correlation of directions from the three sites. Reasonable alternatives to the preferred sequence imply more complicated directional behavior (certainly a possibility during the transitional stage), but retain the near-sided character described above.

Paleomagnetic Directions: N-R

The N-R transition zone occurs in the thick, horizontal flows of the Olokele Formation [*Macdonald et al.*, 1960]. These flows crop out in a roughly circular area in the island's interior and are typically separated from flows of the Napali Formation by well-defined scarps. Both formations are predominantly olivine basalt, and it is clear that the Olokele flows constitute a caldera-filling series that slightly post-dates most of the Napali Formation.

The N-R horizon in the Olokele flows (the "Olokele transition zone") is at nearly the same elevation as the R-N transition in Napali flows at the Kukui Trail site and over 305 m below R-N sites that we located with the flux gate magnetometer nearer the caldera boundary. Our magnetic reconnaissance has shown that a thick section of Napali flows younger than those in the R-N transition zone are normally magnetized, as are all exposed Olokele basalts older than the N-R horizon. Unless an entire reversed magnetozone is missing high in the Napali Formation, it is by far simplest to hypothesize that the N-R reversal recorded in the Olokele flows directly followed the R-N reversal recorded in the Napali flows; that is, the Napali flows above the R-N transition and the Olokele flows below the upper N-R transition belong to the same normal magnetozone. We therefore interpret the R-N and N-R transition zones as recordings of an R-N-R reversal pair.

Our primary site in the Olokele transition zone is at a spot very near the caldera boundary known as Kahililoa (see Figure 1; Appendix A contains a more complete description of the site). In addition to the 26 units sampled at Kahililoa, we took cores from two flows (DG1 and DG2 in Table 4) lower in the section that are exposed about 2 km to the east in the canyon of Koaie Stream.

Collection and laboratory procedures for the samples from the Olokele Formation were identical to those described for the Napali transition zone. The flow-averaged directions and relevant statistics are listed in Table 4 and plotted in Figure 3. Within-flow precision was even greater in the Olokele flows than in the Napali flows; a single flow (OK22) yielded $\alpha_{95} = 0.6°$ [*Fisher*, 1953] for seven samples, and only three flows had values greater than 3.1°.

The sequence of changing field directions at Kahililoa is very similar (except in reverse) to that seen in the Napali flows. The normal direction in DG1 is followed by the northerly and slightly upward direction in DG2. Ten flows (OK1-OK10) with normal but somewhat northeasterly directions follow. The field then steepens while staying northerly; flows OK11 through OK17 yield inclinations close to 72°. A flow with a horizontal ($I = 00.6°$) south ($D = 183.7°$) direction immediately overlies those with the steeply downward directions. In the uppermost flows, the field is seen to shallow to the expected reversed direction. As in the Napali transition, therefore, the field appears to have reversed direction by a downward rotation close to the N-S vertical plane. The correspondingly VGP path passed very near to Kauai. This finding is significant not only because the path is distinctly near-sided, but also because it is so similar to the R-N path obtained from the Napali flows. Another feature common to both records, the sizable gap between the shallow southerly and steep north-

TABLE 4. Kahililoa (Olokele Formation) Directional Results

Flow	Samples	Oe	N	α_{95}	k	D	I	Latitude	Longitude
OK26	8Q043–049	300	7	1.1	2890	188.5	−34.1	−82.0	115.7
OK25	8Q036–042	100	7	1.8	1091	174.0	−34.0	−84.3	292.3
OK24	8Q029–035	100	7	1.7	1264	175.7	−29.0	−84.6	255.1
OK23	8Q022–028	100	7	1.4	1825	161.2	−53.0	−67.8	339.7
OK22	8Q015–021	100	7	0.6	9999	162.9	−54.1	−68.2	344.3
OK21	8Q008–014	200	7	3.1	386	157.1	−58.3	−61.9	345.1
OK20	8Q001–007	200	7	5.8	109	169.6	−38.7	−79.9	313.0
OK19	8Q051–056	100	6	1.9	1193	183.7	00.6	−70.4	193.9
OK18	8Q057–063	···*	···*	···*	···*	···*	···*	···*	···*
OK17	8Q064–070	200	7	1.7	1217	000.8	72.7	50.9	205.7
OK16	8Q071–077	200	7	1.9	1013	350.7	73.7	48.8	197.9
OK15	8Q078–084	200	7	4.2	207	351.0	72.3	51.0	197.3
OK14	8Q085–091	200	7	0.9	4085	350.6	73.2	49.5	197.5
OK13	8Q092–098	200	7	0.7	7682	356.3	71.3	53.0	201.6
OK12	8Q099–105	200	7	1.6	1503	359.6	71.2	53.2	204.6
OK11	8Q106–112	200	7	1.4	1935	002.1	70.1	54.9	207.1
OK10	8Q113–119	400	7	4.2	204	028.7	39.2	63.0	283.2
OK9	8Q120–926	100	8	2.6	466	032.7	35.9	59.2	287.8
OK8	8Q127–133	300	7	2.0	947	031.7	35.8	60.1	288.1
OK7	8Q134–940	100	8	2.6	470	021.8	25.9	68.4	306.1
OK6	8Q141–147	300	7	2.4	616	036.2	30.0	55.4	294.0
OK5	8Q148–154	200	7	2.4	662	035.2	34.5	56.8	289.2
OK4	8Q155–161	200	7	2.8	471	036.4	32.7	55.5	291.0
OK3	8Q162–168	200	7	1.2	2674	035.7	32.2	56.1	291.7
OK2	8Q169–175	200	7	1.8	1120	034.1	34.0	57.8	290.0
OK1	8Q176–182	200	7	1.4	1809	036.5	34.8	55.6	288.6
DG2	9Q315–321	NRM	7	2.5	573	007.6	−06.1	66.7	005.5
DG1	9Q322–328	NRM	7	2.3	688	002.7	27.7	85.0	353.5

For explanation, see Table 1.
*Thermally remagnetized by overlying flow.

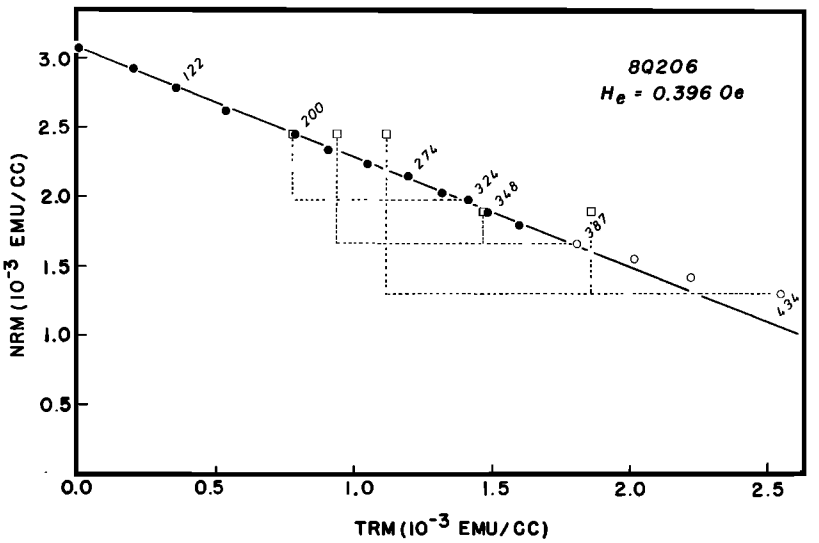

Fig. 4. NRM-TRM diagram showing ideal behavior of sample 8Q206 (Kukui Trail site) at temperatures below 387°C. The straight line is fit to the solid dots only. Dashed lines and squares show repeat of remagnetization steps at 200°C after heating to 324°C, 387°C, and 434°C, and to 348°C after heating to 387°C and 434°C. By 387°C, alteration of the blocking temperature spectrum is apparent.

erly directions, may reflect very rapid field change during the middle portions of both reversals.

Paleointensity Experiments

In preparation for paleointensity experiments on flows from the Napali transition zone, we measured a variety of rock magnetic parameters for about 70% of the samples run. The idea was to eliminate those that might undergo serious alteration during repeated heatings or whose NRM was not a primary TRM in single- or few-domain grains. Acceptable samples generally showed a change in the saturation magnetization (J_s) after heating to 600°C of less than 10% and principal Curie temperatures between 504°C and 573°C. Simple logarithmic extrapolation of a two-week storage test demonstrated that any viscous remanent magnetization (VRM) persisting more than a few seconds was less than 6% of the NRM in all paleointensity samples. Finally, the observed ratios of saturation remanence (J_{rs}) to J_s, between 0.11 and 0.41 for all samples, provide evidence that large multidomain grains do not contribute significantly to the remanance.

Following this preliminary work, we determined ancient field intensities by using the method developed by *Thellier and Thellier* [1959] and modified by *Coe* [1967*a*, *b*]. After measurement of the room temperature (T_r) NRM, a specimen was heated to T_1 and cooled in a magnetic field of less than 100 gammas. This heating demagnetized the component of the NRM residing in the blocking temperature (T_B) interval [T_r-T_1]. The specimen was then heated again to T_1 and cooled in a field of known direction and magnitude (between 0.2 Oe and 0.5 Oe). The vector difference before and after heating defined the partial TRM (PTRM) acquired in the interval [$T_r - T_1$]. This procedure was repeated to progressively higher temperatures until the sample was completely remagnetized or until it appeared that all unaltered portions of the T_B spectrum had been examined. The heating–cooling cycles, each several hours long, were performed in a vacuum of approximately 10^{-5} torr.

The graphical method of *Arai* [1963] is the most convenient way to display the results of the Thelliers' experiment. By this method, the intensity of the NRM remaining after each heating step is plotted against the TRM gained up to that point. As an example, consider sample 8Q206 (Figure 4). The first 12 points on the NRM-TRM diagram form a well-defined straight line segment; the associated temperatures range from room temperature (020°C) to 370°C. After the demagnetization heating to 387°C, a repeat determination of the PTRM acquired at 200°C showed that alteration in the low-temperature portion of the blocking temperature spectrum had begun. The NRM-TRM points beyond 387°C deviate

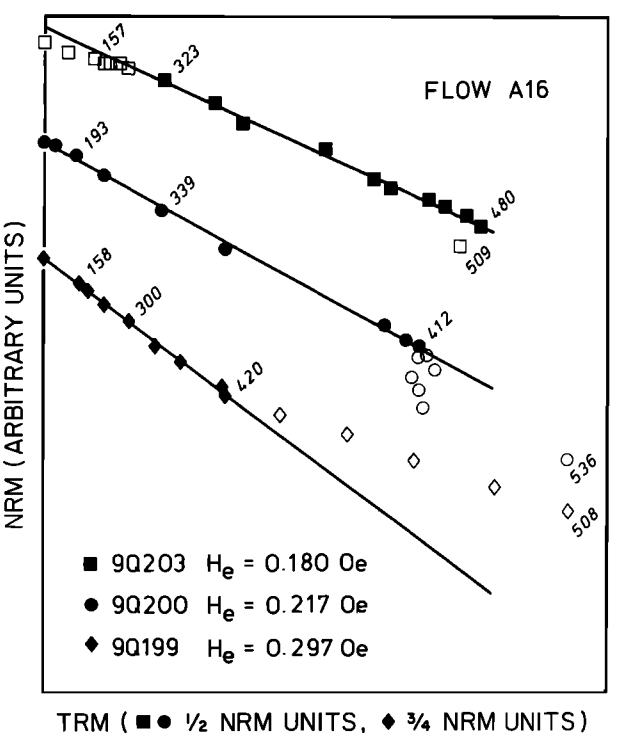

Fig. 5. NRM-TRM diagram for three samples from flow A16. Straight lines are fit to the solid symbols only. TRM units are adjusted for differences in the laboratory field H_L (for 9Q203 and 9Q200, H_L = 0.2 Oe; for 9Q199, H_L = 0.3 Oe) so that the slopes are directly comparable.

TABLE 5. Paleointensity Results

Flow	Sample	N	$[T]$	Ang.	f	σ_b/b	q	H_e	$\bar{H}_e$
KT32	8Q184	6	020–302	1.7	0.224	0.0220	8.0	0.448	0.444
KT32	8Q189	11	151–446	2.6	0.425	0.0382	10.0	0.442	(±0.003)
KT30	8Q202	5	156–287	2.8	0.185	0.0441	3.0	0.445	0.443
KT30	8Q203	7	156–343	2.3	0.184	0.0720	2.1	0.440	(±0.003)
KT29	8Q206	12	020–370	3.9	0.415	0.0121	31.0	0.396	0.368
KT29	8Q207	6	078–288	1.4	0.258	0.0640	3.1	0.380	(±0.016)
KT29	8Q208	7	078–322	1.5	0.376	0.0106	28.2	0.342	
KT28	8Q211	10	074–344	0.8	0.149	0.0395	3.3	0.360	0.378
KT28	8Q214	11	073–429	2.4	0.528	0.0117	39.8	0.373	(±0.009)
KT28	8Q217	8	020–372	2.3	0.457	0.0137	28.0	0.390	
KT26	8Q227*	7	348–479	1.8	0.241	0.0451	4.0	0.310	0.293
KT26	8Q228*	7	346–479	1.4	0.244	0.0501	3.7	0.293	(±0.021)
KT26	8Q229*	4	373–433	1.2	0.117	0.0947	0.8	0.227	
KT26	8Q230*	6	377–482	1.3	0.147	0.0496	2.2	0.266	
KT23	8Q246	6	449–531	0.4	0.137	0.0302	3.5	0.231	0.218
KT23	8Q247	9	411–529	2.0	0.270	0.0253	8.1	0.205	(±0.014)
KT23	8Q252	4	453–514	0.4	0.248	0.0575	2.7	0.248	
KT18	8Q282*	5	442–520	2.2	0.160	0.0267	4.4	0.296	0.292
KT18	8Q286*	5	380–475	1.8	0.160	0.0777	1.5	0.259	(±0.022)
KT18	8Q287*	4	417–458	0.8	0.074	0.0789	0.7	0.333	
KT13	8Q318*	8	314–477	3.0	0.337	0.0551	5.1	0.304	0.301
KT13	8Q319*	6	371–499	0.8	0.364	0.0541	4.8	0.311	(±0.004)
KT13	8Q322*	7	369–491	4.0	0.353	0.0281	10.0	0.298	
KT9	8Q345*	4	309–407	0.5	0.149	0.0545	1.8	0.496	0.431
KT9	8Q349*	5	372–472	0.7	0.188	0.0322	4.2	0.422	(±0.046)
KT5	8Q372	11	407–558	0.4	0.578	0.0112	42.9	0.344	0.348
KT5	8Q376	11	196–493	2.0	0.304	0.0253	10.6	0.476	(±0.052)
KT5	8Q378	10	245–474	1.5	0.317	0.0440	6.1	0.347	
A16	9Q199	9	020–420	3.8	0.314	0.0222	12.0	0.297	0.217
A16	9Q200	9	020–412	2.6	0.468	0.0168	21.3	0.217	(±0.036)
A16	9Q203	10	323–480	1.6	0.322	0.0261	10.6	0.180	
A7	9Q143*	5	388–444	7.0	0.143	0.0260	4.0	0.099	0.101
A7	9Q144	5	157–348	6.1	0.227	0.0521	3.3	0.104	(±0.003)
A7	9Q146	4	156–301	2.1	0.099	0.1476	0.4	0.107	
A5	9Q132*	5	325–434	4.1	0.120	0.1420	0.6	0.117	0.111
A5	9Q134*	5	325–433	1.9	0.151	0.0467	2.3	0.111	(±0.004)

N and $[T]$ are the number of NRM-TRM points and temperature interval used for the paleointensity determination. Ang. is the angular change in the NRM direction through $[T]$. The f, σ_b/b, and q are the NRM fraction, normalized standard error of the slope, and quality factor of *Coe et al.* [1978]. H_e and $\bar{H}_e$ are the sample and flow-mean paleointensity in Oe, with the standard deviation of the flow-mean paleointensity [*Coe et al.*, 1978] in parentheses.

*Result from nonideal NRM-TRM curve.

from the lower temperature trend, and we therefore used only the first twelve points to estimate the ancient field intensity for this sample.

The specimens from flows KT32, KT30, KT29, KT28, KT23, KT5, A16, and A7 (except 9Q143) all yielded NRM-TRM diagrams similar to that for 8Q206. Figure 5, for example, shows well-defined, straight line segments for the three samples from A16, a flow that will be critical in the discussions that follow. In these and many other NRM-TRM diagrams, a few of the lowest temperature points lie above or below the linear trend of the higher temperature points, an effect undoubtedly due to VRM. Nevertheless, the central portions of the NRM-TRM plots for these samples are characterized by straight line segments, consistency in the estimated ancient field intensity between samples, and the apparent lack of alteration at temperatures below those spanned by the straight line segment. These three characteristics are strong evidence that the NRM-TRM behavior of the samples reflects the ancient field intensity with reasonable accuracy. We list sample numbers, parameters describing each experiment and final results in Table 5.

In a second group of specimens, primarily from flows KT26, KT18, KT13, KT9, and A5, nonideal behavior occurred during the early stages of the heatings. The NRM-TRM diagrams of the samples from flow KT13 (Figure 6) provide examples: The nonideal behavior is apparent as a downward "kink" in the NRM-TRM curve that begins near 200°C and continues until after 300°C. The kink represents a drop in NRM intensity that is not fully compensated by the TRM gain. In the group of samples discussed above, this kink is either not present (13 samples) or occurs after a well-defined linear segment at lower temperature (eight samples). In the remaining samples, however, there is no clearly defined linear segment preceding the kink. The problem then is whether the

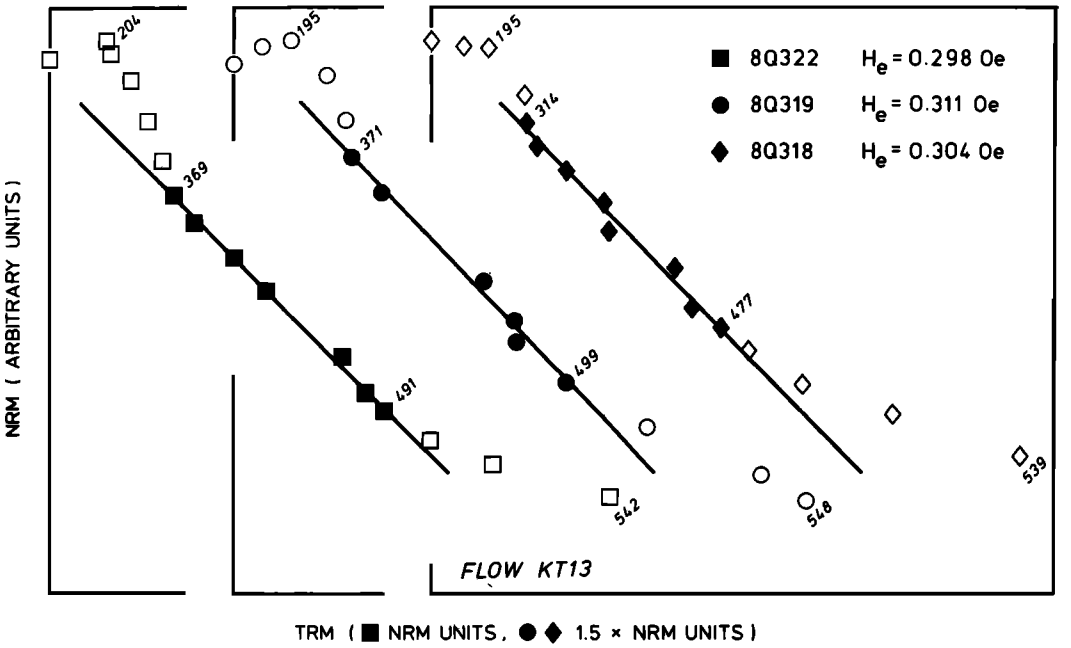

Fig. 6. Nonideal NRM-TRM diagrams for three samples from flow KT13. The lines are fit to the solid symbols, and the TRM units adjust for differences in the laboratory field. The first 200°C of heating removes a present field component roughly antiparallel to the reversed remanence in the samples. Between 200° and 314° to 371°, a downward "kink" in the trend of the NRM-TRM data is apparent. Despite this nonideal behavior, the paleointensities derived from the three samples are in excellent agreement.

slope of the linear segment following the kink can be taken as a measure of the ancient field intensity. This question is by no means trivial; if the kink signals alteration of the T_B distribution, then a fundamental requirement of the Thelliers' paleointensity technique has been violated.

Although a definitive answer to the above question is not possible, there are three kinds of internal consistency that give us a degree of confidence in the paleointensities inferred from the post-kink segments. At the within-specimen level, the linearity of points (i.e., the consistency of slope) in the segments suggests that alteration did not seriously affect the crucial portion of the T_B spectrum. There is also good agreement between samples from individual flows. Samples from flow A7, for example, give paleointensity estimates from both pre-kink (two samples) and post-kink (one sample) segments that agree to within 8%. Similar consistency is seen in flows where the only interpretable linear segments occur after kinks. Flow KT13 (Figure 6) provides a spectacular example; the paleointensity estimates from three samples agree to within 4%.

Finally, there are two samples (8Q184 and 8Q208) that clearly show linear segments both before and after the kink. In both cases we use the lower temperature points when calculating the paleointensity for the sample. Of interest here is that the pre-kink and post-kink segments on the two NRM-TRM diagrams have similar slopes. The first sample (8Q184) yields a paleointensity of 0.448 Oe from the lower temperature segment and of 0.460 Oe from the higher temperature segment. Sample 8Q208, from a different flow, gave corresponding values of 0.342 Oe and 0.305 Oe. These within-specimen discrepancies are not large; they amount to errors of 3% and 12%, respectively, and are of the same order as those often found between ideal samples from the same flow. It is also important that the lower temperature paleointensity estimate from 8Q184 is less than that derived at higher temperature, while for 8Q208 the opposite is true. There is thus no reason to suspect a systematic bias to results derived from the second linear segments.

In general terms, the kinks signal the transfer of remanence or TRM capacity from low to high temperature portions of the T_B distribution. The internal consistency described above suggests that this transfer can sometimes occur without seriously affecting the remanence in grains with intermediate T_B's. Possible mechanisms for this nonideal behavior include the disproportionation of minor titanomaghemite [e.g., *Coe et al.*, 1978] or partial oxidation of low T_B titanomagnetite [e.g., *Prévot et al.*, 1983]. Alteration of this kind during paleointensity experiments on basalts from Hawaii [*Coe et al.*, 1978], caused a progressive drift of the NRM direction in a sample toward the applied TRM. In contrast, the NRM direction in the Kauai samples remained quite stable through the critical range of temperatures. If drift did occur, it was not until an increase in the TRM capacity was already apparent in the NRM-TRM plot. It is also curious that neither the J_{rs}/J_s ratio nor the reversibility of $J_s - T$ curves seemed to correlate with the occurrence of nonideal behavior. Our understanding of the process giving rise to the kinks is far from complete, and for now confidence in the paleointensity estimates from nonideal samples depends heavily on the internal consistency arguments.

Paleointensity Results

Table 5 lists the results of paleointensity experiments on 36 samples from 13 flows in the Napali transition zone. Of these 36, 28 are from the Kukui Trail site and eight are from Anahola. Six additional samples were studied but yielded highly nonideal NRM-TRM diagrams. We used a generalized least-squares method [*Coe et al.*, 1978] to fit lines to the NRM-TRM data. All points within the selected temperature range were included for the line fitting procedure. We also calculated a quality factor for each specimen, a weighted average of specimens within each flow, and a generous estimate (i.e., larger than orthodox) of the standard deviation of the flow mean as described by *Coe et al.* [1978]. None of the rock-magnetic parameters measured prior to the start of the pa-

leointensity experiments showed an obvious correlation with either the quality factor or precision of the paleointensity results.

Figure 7 shows how flow-averaged field intensity varies through the transition zone in the Napali Formation. The basis for points on the horizontal axis is the lava flow stratigraphy at the Kukui Trail site. Flows with very similar directions or combined directions and paleointensities are grouped together, and points are included for flows A5, A7, and A16 from Anahola according to the correlation of flows between the sites that we prefer. Thus, assuming that groups of flows with very similar remanence directions are the result of quick eruptive pulses, each point along the abscissa is roughly equivalent to an instant of time. Spaces between the points represent intervals of time long enough for a change in the geomagnetic field direction or intensity to occur. A plot of intensity against such an axis shows the variation of intensity versus time at least as well as a plot versus flow number or stratigraphic height, though it is not possible to estimate how good the approximation of time is.

In the Napali transition zone, paleointensity drops from 0.431 Oe to 0.101 Oe and rises again to 0.444 Oe. Thus, the reversal is characterized by a 77% drop in field intensity. The overall pattern of the intensity variation versus "time" is V shaped; a steady rise follows a steady decline, with only a relatively short interval of minimum intensity. In this respect, the reversal record from Kauai resembles the variation of NRM intensity in the Olduvai-Matuyama record in Indian Ocean sediments [*Opdyke et al.*, 1973] and in the Matuyama-Brunhes records from Lake Tecopa [*Hillhouse and Cox*, 1976] or the central Pacific [*Kawai et al.*, 1976]. In contrast, the transition zones in clays from Crete [*Valet and Laj*, 1981] or the Tatoosh intrusion [*Dodson et al.*, 1978], or those reported from Russian sites [*Petrova et al.*, 1972; *Kaporovich et al.*, 1966] show an extended interval of reduced NRM intensity. If one presumes that NRM intensity is proportional to the ancient field intensity, then the drop in apparent field intensity from the latter examples is greater than the drop in paleointensity seen in the Napali flows. The problems of averaging in

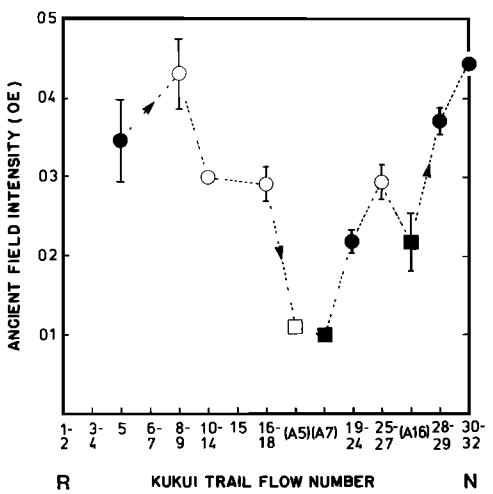

Fig. 7. Ancient field intensity through the Napali transition zone. Flows with similar direction or direction and intensity are grouped together on the abscissa. Each point thus represents an interval of time that is short with respect to the geomagnetic variation; the true time interval between points is not known. Circles (squares) denote results from the Kukui Trail (Anahola) site; open symbols mean that the paleointensity is based only on nonideal NRM-TRM diagrams. Vertical bars show standard deviations of the flow-mean paleointensities (if greater than height of symbols).

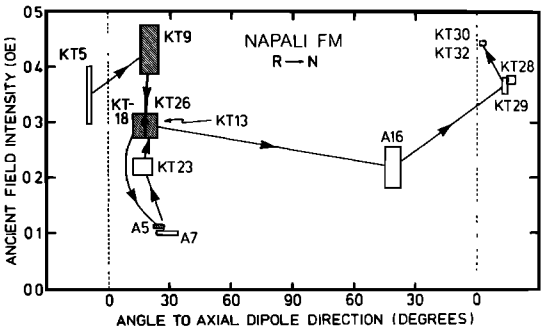

Fig. 8. Flow-averaged paleointensity versus angle to the axial dipole directions through the Napali transition zone. Directions equivalent to near-sided VGP positions (i.e., shallow southerly or steep northerly directions) plot between the dashed lines. Height and width of box shows the standard deviation of the mean paleointensity and the α_{95} of the mean direction for each flow. Hatched data are based entirely on samples that exhibited nonideal behavior in the Thelliers' experiment.

sediments and the possibility of incomplete sampling by lava flows make it unwise to ascribe too much significance to this difference, however.

Notice that the paleointensity reached its minimum with flows A5 and A7 (Figure 7), whereas the majority of the direction change occured later between flows KT26 and A16 (Figures 2 and 3). There was 68% recovery of intensity as the field direction moved back closer to the reversed axial dipole direction after flows A7 and A5. Unfortunately, it is not possible to know whether the field intensity again dropped or remained high during the stage of major direction change between KT26 and A16. The only clue is that by the time of A16, the field strength was at 0.217 $\pm$ 0.036 Oe. Because this is significantly lower than the intensity from KT26 (0.293 $\pm$ 0.021 Oe), it seems most likely that field strength did drop again before final recovery. An alternative correlation, with flows A5 and A7 placed after KT26, would make the intensity variation simpler but, as described earlier, imply more complicated directional behavior.

One way to sidestep the uncertainty just described, and that of not knowing the time interval between neighboring flows, is to restrict attention to the relationship of intensity and directional changes during the transition. This aspect of the reversal record is summarized in Figure 8, where paleointensity is plotted versus angle between the NRM and the axial dipole direction. The data yield no information on the intensity behavior within the central portion of Figure 8, a phase of the reversal that, as mentioned above, may have occurred quite rapidly. What the data do provide is a view of two other important parts of the reversal: the decay of the reversed field and the final approach to normal polarity.

Systematic differences between the initial and final stages of the transitional field have been observed [*Fuller et al.*, 1979; *Clement and Kent*, 1983] and proposed on theoretical grounds [*Hide*, 1981]. The data in Figure 8 are consistent with an assymmetry of this sort. Directional stability and large intensity changes characterized the decaying reversed field. More specifically, a 77% drop and partial recovery of the field strength occurred while the direction remained within 30° of the axial dipole direction. The intensity pattern for the conclusion of the reversal is not as well constrained. Nevertheless, the relatively high paleointensity of A16 and the trend of increasing paleointensity through flow KT32 suggest a gradual recovery of field intensity that began while the direction was

still transitional. In the following section, we speculate on the implications of this difference for two simple reversal models that are equally capable of explaining the directional results.

COMPARISON TO REVERSAL MODELS

The most striking feature of the field directions recorded in the R-N and N-R transition zones on Kauai is their similarity; the VGP paths for both reversals probably passed near the site. As we have discussed elsewhere [*Bogue and Coe*, 1982], the recurrence of intermediate field directions in successive reversals is consistent with the idea of *Hillhouse and Cox* [1976] that a standing, nondipole field component persists through the decay and regrowth of the main dipole field and controls the field direction at the intermediate stage. This model of transitional field behavior, referred to as the standing field model, predicts identical sequences of transitional field directions for repeated reversals as viewed from a single site. The paleomagnetic results from three transition zones in California [*Hillhouse and Cox*, 1976; *Mankinen et al.*, 1981; *Liddicoat*, 1982] support such a model and further require the postulated standing field to persist for several million years.

Valet and Laj [1981] provide conflicting evidence from clays of Miocene age in Crete. The sequence of field directions they obtained from an R-N transition zone is grossly dissimilar to that from the succeeding N-R horizon 9 m upsection; the equivalent VGP paths are 135° apart longitudinally near the equator. Clearly, these data cannot be reconciled with the standing field model unless (1) the standing field sometimes changes relatively rapidly or (2) other effects are sometimes more important in controlling the intermediate stages of the reversing field. The latter possibility implies that the standing field may only be observable as a site-dependent directional bias when comparing many reversal records.

This general conclusion does not preclude the possibility that a standing field is responsible for the very similar sequences of directions seen in the Kauai transition zones. The sequences from the Napali and Olokele Formations require a standing field vector with declination close to 0° or 180°. To produce the nearly vertical downward direction seen in both sections, the vector must also have had a component directed perpendicularly (in the south-down sense) to the expected normal or reversed direction.

Paleointensity information allows one to be even more specific about the field component postulated to control the transitional directions. In the Napali transition zone, the ancient field intensity decreased from 0.431 Oe to 0.101 Oe while the field was still within 30° of the expected reversed direction. In a standing field model, this pattern of intensity change could only occur if (1) the standing field component was very small or if (2) the component was at a small angle to the axial dipole direction. A problem arises, however, because a larger or more perpendicularly oriented nondipole component is required to explain the field behavior during the final stage of the reversal. As shown in Figure 9, a plot of intensity versus angular deviation for any particular standing field model is quite symmetrical except for differences in the starting and final field intensities. The important point is that the standing field model cannot explain an asymmetric intensity pattern like that suggested by the paleomagnetic data from Kauai.

The transitional sequences from Kauai are both characterized by directions that lie near the north–south vertical plane. Similar behavior arises in the zonal reversal model of *Hoffman* [1977, 1979] in which the earth's fluid core is treated as a distributed source of magnetic field. Hoffman hypothesizes that polarity transitions begin with a localized reversal of field sign in a small region of the core, an effect that then spreads, or "floods," through the remainder of the source region. At intermediate stages, higher order fields will predominate, and if the source region retains zonal symmetry, the transitional field will be a sum of axial multipoles. The simplest cases are those in which flooding begins at a pole or along the equatorial band of the fluid core. The former results in a predominantly quadrupolar transitional field, and the latter results in an octupolar field at the midpoint of the reversal.

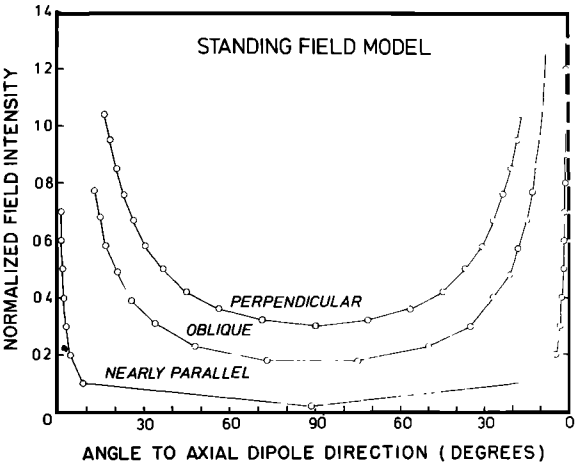

Fig. 9. Field intensity versus angle to the axial dipole direction for the standing field model. Curves are drawn for a constant field vector in the N-S vertical plane with magnitude 0.3 that is perpendicular, oblique (35°), or nearly parallel (3°) to a stationary dipole vector with magnitude varying between 1.0 and −1.0.

Directional data from transition zones suggests that flooding processes (if important in controlling the transitional field) must sometimes change between reversals [*Bogue and Coe*, 1982; *Williams and Fuller*, 1982]. This possibility has important implications for the way one applies Hoffman's model. *Hoffman and Fuller*'s [1978] method for determining the origin point of flooding involves the comparison of paleomagnetic records of both R-N and N-R reversals. Such a test will be inconclusive or misleading if different flooding schemes are operating for the reversals under consideration. This kind of difficulty is of course avoided when applying the model at the level of a single reversal, but paleomagnetic directions alone are not very revealing; the standing field and zonal flooding models, octupolar or quadrupolar, are equally capable of generating near-sided VGP paths like those from Kauai.

As was the case with the standing field model, it is more informative to compare the predictions of zonal flooding models to fully vectorial data. For this purpose we use a roughly spherical magnetic source that is similar in concept to the cylindrical models described by *Hoffman* [1977, 1979]. The spherical source, described in more detail in Appendix B, comprises 14 latitudinal zones each containing a ring of point dipoles. Reversals are simulated by reversing the polarity of each zone in sequence. The most important differences between the transitional fields predicted by this model and those of Hoffman are the minimum field intensities that depend critically on geometry of the model source at mid-transition. Figure 10 shows the paleointensity results from Kauai with the octupolar and quadrupolar model curves appropriate for 19°N. We have plotted the component of the transitional field vector that lies in the north–south vertical plane; that is, the

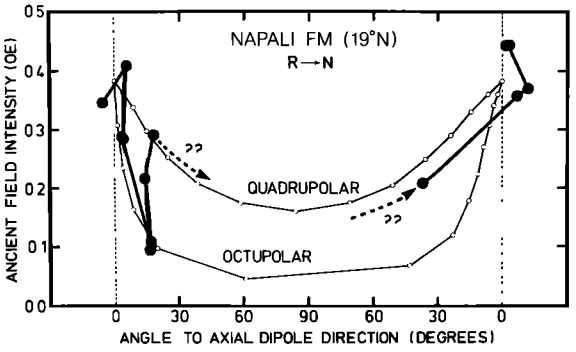

Fig. 10. Comparison of paleointensity variation (axial component only, shown as large dots) in the Napali transition zone with that predicted by quadrupolar and octupolar zonal flooding models. Reversal initiates at the south end of the fluid core for the quadrupolar model and at the core equator for the octupolar model. The initial model field intensity (0.38 Oe) is consistent with the mean paleomagnetic dipole moment for the past 5 m.y. calculated by *McFadden and McElhinny* [1982]. Data between the dashed lines correspond to near-sided VGP positions.

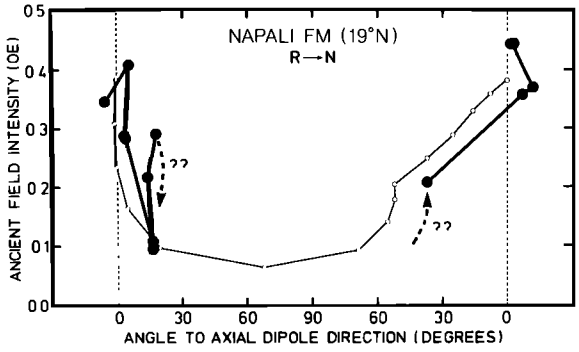

Fig. 11. Comparison of paleointensity variation (axial component only, shown as large dots) in the Napali transition zone with that predicted by the "best-fit" zonal flooding model. Reversal initiates just north of the core equator, floods first to the south and then to the north. The initial model field intensity is the same as in Figure 10. Data between the dashed lines correspond to near-sided VGP positions.

component that can be explained by a strictly zonal model. The projection adjusts the points only slightly (compare Figures 8 and 10) because the paleomagnetic directions all lie near the projection plane to begin with. The model curves are drawn with a starting field intensity of 0.38 Oe, a value consistent with the mean dipole moment of 8.535×10^{25} emu estimated by *McFadden and McElhinny* [1982] for the past 5 m.y.

As can be seen in Figure 10, the results from Kauai fit neither the octupolar nor the quadrupolar model and, instead, exhibit characteristics of both. A primary feature of the octupolar model is that the intensity drops sharply before the field direction undergoes much change; this pattern also characterizes the paleointensities and directions from the Napali flows at the base of the transition zone. The quadrupolar model, on the other hand, predicts that the intensity will change more gradually as the direction moves toward or away from intermediate positions. This style of change resembles the pattern sketched by data from the top of the Napali transition zone.

One way to accommodate these observations is to suppose that very different flooding schemes can operate during a single reversal episode. The initial decrease and partial recovery of the intensity seen in the Kauai data may thus represent an aborted attempt by the field to reverse by flooding from the equatorial zone. A similar mechanism could explain the direction for flow KT15 and, as discussed by *Hoffman* [1981], the properties of geomagnetic excursions. Following a return toward the initial reversed state, flooding may have begun again in a different region, near the south pole of the core, and continued through to completion. The main transitional field would thus have been quadrupolar in character, implying that during the time between flows KT26 and A16, the field intensity did not again get as low as observed in flows A5 and A7. The picture that emerges from this line of speculation is that of an unstable core system that is ready to reverse, but with no strong preference for one flooding scheme over another.

It is also possible to model the asymmetric intensity pattern recorded in the Kauai flows by using a flooding mechanism that is itself asymmetric. One such scheme, described in more detail in Appendix B, is roughly equivalent to having the reversal flood northward and southward, but at very different rates, from an initiation point near the core's equator. In its early stages, this model resembles the octupolar model because the equatorial zone reverses first; a large drop in intensity precedes the direction change (see Figure 11). With continued flooding, the transitional field becomes increasingly quadrupolar in character. As the reversal nears completion, the normal field direction is approached gradually while field intensity is relatively high. The agreement of this model with the results from the Napali transition zone, also shown in Figure 11, is quite good. Thus, while both the standing field and zonal flooding models can explain site-dependent reversal paths, the zonal flooding model alone can give rise to asymmetry consistent with the paleointensity data. To be viable, other reversal models must also have this capability.

APPENDIX A: SAMPLE LOCALITIES

Kukui Trail Site (22.06°N, 200.35°E)

The Kukui Trail leads down into Waimea Canyon from the Kokee road and is where *Doell* [1972] collected normally magnetized samples. The transition zone is below Doell's lowest site on the trail, just south and uphill from the saddle at 561 m (1840 ft). Basalt flows crop out in a dry and brushy watercourse that parallels the upper half of the trail. We sampled about 31 m of section between elevations of 573 m (1880 ft) and 604 m (1980 ft). The horizontal distance up the sampled section in the creek bed is approximately 100 m.

Basalts of the Napali Formation are exposed from the top of the trail down to the saddle. At the saddle, the trail turns northward and follows a brecciated zone that separates Napali Formation on the west from a small pod of later graben-filling flows of the Makaweli Formation [*Macdonald et al.*, 1960]. From a point on the trail about 400 m west of the saddle, a large dike can be seen to cut across the gully in which the transition zone is exposed. Examination of a few samples with a portable magnetometer showed the dike to be normally magnetized. The dike follows a more easterly trend than the gully itself, and at the level of the transition zone the dike is 60–90 m south of the sampling site. Several large pieces of the dike that broke off and washed down the creek bed are visible in the sampling area. We inadvertently sampled a large block of this float ("flow" KT20) that was partially exposed in the floor of the gully.

Anahola Site (22.16°N, 200.67°E)

The second site in the Napali transition zone is west of Highway 56, about 2.4 km north of the town of Anahola. The

site is located on the southeast flank of the small peak (342 m or 1121 ft) that lies about 800 m west of the point where Aliomanu Road joins the highway. The lowermost flows that we sampled are at the 122-m (400-ft) elevation in an intermittent stream that trends ENE-WSW and cuts into the eastern side of the peak. Flows are exposed all the way to 342 m (1121 ft), but we sampled only to 274 m (900 ft) because of problems with lightning strikes, as explained in the text.

Geologically, the site at Anahola is an erosional remnant of the Napali flows that once formed the eastern half of the main volcanic shield. Weathering and erosion, which are much more intense on windward Kauai than to the west, have removed much of the surrounding Napali rocks. A younger episode of resurgent volcanism [*Macdonald et al.*, 1960] has served to further isolate the Anahola site.

Polihale Site (22.10°N, 200.26°E)

We sampled approximately 27 m of section near the 183 m (600 ft) elevation on the northwest-facing nose of Polihale Ridge, about 800 m north of Polihale State Park. At this locality, and to the northeast, Napali flows are very well exposed in the steep sea-cliffs that form Kauai's Napali coast. To the north of Polihale, access for sampling is difficult because the transition zone gets higher in the cliffs. The first site to the north where the R-N horizon is easily reached from above is at 463 m (1520 ft) above Miloii State Park.

Kahililoa Site (22.09°N, 200.35°E)

The primary sampling site in the Olokele transition zone is at the southwest end of Kohua Ridge, on the south and west facing sides of Kahililoa. This prominent point (elevation 854 m, or 2803 ft) is situated at the confluence of the Waimea River and Koaie Stream in the northern end of Waimea Canyon. We originally located the site on a traverse down from the end of the jeep trail on Kohua Ridge, but it can also be reached from below on the Koaie Stream side. The highest flow we sampled is at 695 m (2280 ft) and the lowest is at 579 m (1900 ft). The section thus comprises nearly 120 m of Olokele basalt flows.

Kahililoa is very near the caldera boundary. Makaweli flows occur 60–90 m below the lowest flow that we sampled, and Napali flows are exposed to the west across the Waimea River.

We also sampled two flows at 457 m (1500 ft) and 451 m (1480 ft) in the dry gulch that leads off to the northwest from the 433 m (1420 ft) elevation on Koaie Stream. The reason for sampling at this site (22.10°N, 200.37°E), which is well within the caldera, was to get lower in the Olokele section than was possible at Kahililoa because of the contact with the Makaweli Formation.

APPENDIX B: ZONAL REVERSAL MODEL

To approximate the geomagnetic source, we divide the fluid core into a series of 20 zones, each aligned perpendicularly to the earth's rotation (z) axis. Point dipoles situated in these slices constitute rings about the z axis; collectively they form a roughly spherical source of dipole and higher order magnetic field. We constrain the dipoles to lie halfway between the boundaries of the inner and outer cores, and as a consequence they will be present only in the middle 14 of the 20 slices. Table B1 lists the volume and displacement h along the z axis for each slice containing a dipole ring of radius x.

Consider a ring of point dipoles, where the axis of the ring and each point dipole are aligned parallel to the z axis (Figure B1). It is easy to show [*Bogue*, 1982] that a ring of total dipole moment M and radius x and at height h along the z axis (positive northward) gives rise to a magnetic potential described by zonal spherical harmonic coefficients

$$g_1 = \frac{M}{a^3}$$

$$g_2 = \frac{2Mh}{a^4}$$

$$g_3 = \frac{6Mh^2 - 3Mx^2}{2a^5}$$

$$g_4 = \frac{-6Mhx^2}{a^6}$$

where a is the radius of the earth.

For calculating transitional fields, we made the total dipole moment of each ring proportional to the volume of the correponding fluid core slice and then normalized all coefficients so that the dipole terms sum to 1. These values can be found in the rightmost columns of Table B1. We list the value of g_4 to show that it is never large in comparison with the first three

TABLE B1. Geometry and Magnetic Potential of Slices of Model Core

Latitude	Offset	Radius	Volume	g_1	g_2	g_3	g_4
40.5	2255.5	708.0	7.512	0.052	0.037	0.019	−0.001
33.4	1908.5	1395.0	9.180	0.063	0.038	0.012	−0.005
26.7	1561.5	1774.9	10.419	0.072	0.035	0.005	−0.008
20.5	1214.5	2028.2	11.285	0.078	0.030	−0.003	−0.009
14.5	867.5	2199.1	11.567	0.080	0.022	−0.010	−0.008
8.6	520.5	2306.0	11.408	0.078	0.013	−0.014	−0.005
2.9	173.5	2357.6	11.314	0.078	0.004	−0.016	−0.002
−2.9	−173.5	2357.6	11.314	0.078	−0.004	−0.016	0.002
−8.6	−520.5	2306.0	11.408	0.078	−0.013	−0.014	0.005
−14.5	−867.5	2199.1	11.567	0.080	−0.022	−0.010	0.008
−20.5	−1214.5	2028.2	11.285	0.078	−0.030	−0.003	0.009
−26.7	−1561.5	1774.9	10.419	0.072	−0.035	0.005	0.008
−33.4	−1908.5	1395.0	9.180	0.063	−0.038	0.012	0.005
−40.5	−2255.5	708.0	7.512	0.052	−0.037	0.019	0.001
Total				1.002	0.000	−0.014	0.000

Latitude measured on surface of outer core boundary for slice at height h from equatorial plane and at radius x from axis, with h and x in km. Fluid core slice volume in $km^3 \times 10^9$.

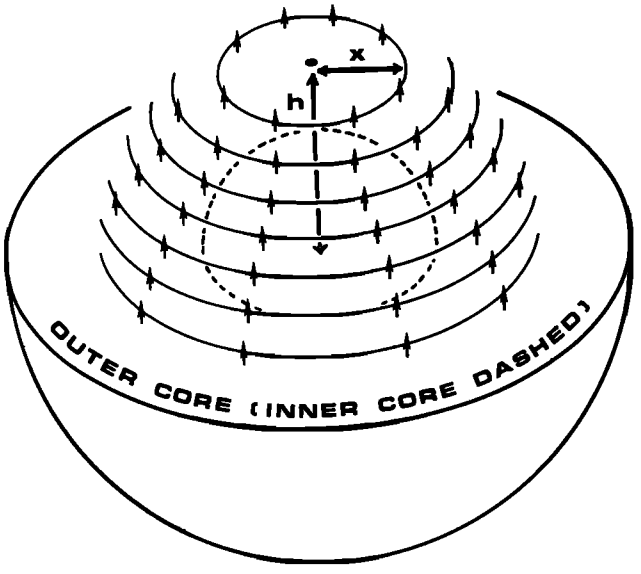

Fig. B1. Side view of model geomagnetic source. Dipole rings (with radius x and height h) constitute a roughly spherical shell halfway between the inner core and the core-mantle boundary. Reversals are simulated by reversing the polarity of the rings in sequence.

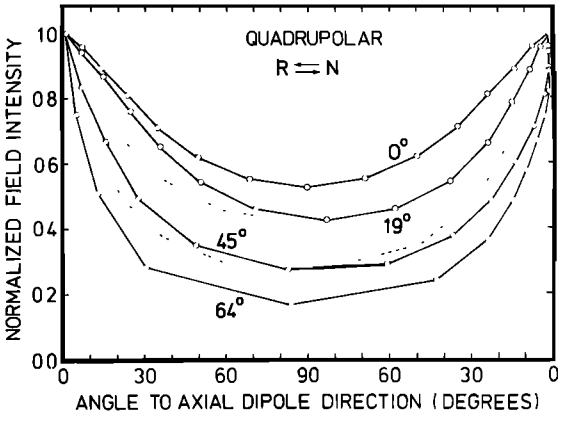

Fig. B2. Normalized field intensity versus angular deviation of field direction for the quadrupolar zonal flooding model. If flooding for an R-N reversal initiates at the north (south) end of the fluid core, then solid lines are for northern (southern) hemisphere sites and dashed lines are for southern (northern) hemisphere sites. The VGP paths are far (near) sided. Notice that minimum field intensity varies considerably with site latitude.

terms. Because the contribution of higher order terms to the surface field is small, only the dipole, quadrupole, and octupole terms are used in the calculations below.

Reversals occur in the model by changing the sign of the potential due to each slice of the fluid core in turn. If the reversal begins in the northernmost slice and proceeds to the south, then a quadrupolar field will dominate the intermediate stages. This can be seen in Table B2, where the totals of g_1, g_2, and g_3 are listed for each stge of this flooding scheme. For comparison with the models of *Williams and Fuller* [1981], total magnetic energy external to the core (dipolar, quadrupolar, and octupolar only) decreases by 61% in this quadrupolar reversal model. Early in the process, up to 7% of the energy is shifted to the octupolar term. The maximum in the quadrupolar energy (19%) occurs when the dipole is zero.

A second possibility is that the reversal initiates in the equatorial slices and floods both southward and northward. The terms for the transitional field generated by this flooding scheme are listed in the middle three columns of Table B2. At the midpoint of the reversal the octupolar component predominates, reaching a maximum of 24% of the initial magnetic energy. Total magnetic energy decreases to a low of 20% slightly earlier in reversal.

Figures B2 and B3 are plots of normalized field intensity versus angle between the field direction and the starting normal or reversed direction for these simple cases. When the transitional field is predominatly quadrupolar, the minimum field intensity varies considerably with the latitude of the site (Figure B2). At the equator, the intensity drops by slightly less than 50%; at 64°N the drop is 83%. In contrast, minimum field strength is essentially invariant with latitude in the octupolar model, near 17% over much of the surface of the earth (Figure B3).

Finally, the rightmost column of Table B2 shows the zonal coefficients for the asymmetrical flooding scheme that best models the paleointensity results from the Napali Formation. The reversal begins in the slice at 8.6°N and floods to the south. Only after the entire southern hemisphere of the core is reversed does the flooding begin to propagate northward from the zone of initiation. The resulting transitional field is at first octupolar and then quadrupolar. Total magnetic energy reaches a minimum of 20%. A maximum of 24% appears in

TABLE B2. Sequences of Transitional Fields

	Quadrupolar Model			Octupolar Model			Kauai Best-Fit		
n	g_1	g_2	g_3	g_1	g_2	g_3	g_1	g_2	g_3
1	1.002	0.000	−0.014	1.002	0.000	−0.014	1.002	0.000	−0.014
2	0.898	−0.074	−0.052	0.846	0.000	0.018	0.846	−0.026	0.014
3	0.772	−0.150	−0.076	0.690	0.000	0.050	0.690	−0.034	0.046
4	0.628	−0.220	−0.086	0.534	0.000	0.078	0.534	−0.026	0.078
5	0.472	−0.280	−0.080	0.378	0.000	0.106	0.378	0.000	0.106
6	0.312	−0.324	−0.060	0.218	0.000	0.126	0.218	0.044	0.126
7	0.156	−0.350	−0.032	0.058	0.000	0.146	0.062	0.104	0.132
8	0.000	−0.358	0.000	−0.098	0.000	0.152	−0.082	0.174	0.122
9	−0.156	−0.350	0.032	−0.254	0.000	0.158	−0.208	0.250	0.098
10	−0.312	−0.324	0.060	−0.398	0.000	0.148	−0.312	0.324	0.060
11	−0.472	−0.280	0.080	−0.542	0.000	0.138	−0.472	0.280	0.080
12	−0.628	−0.220	0.086	−0.668	0.000	0.114	−0.628	0.220	0.086
13	−0.772	−0.150	0.076	−0.794	0.000	0.090	−0.772	0.150	0.076
14	−0.898	−0.074	0.052	−0.898	0.000	0.052	−0.898	0.074	0.052
15	−1.002	0.000	0.014	−1.002	0.000	0.014	−1.002	0.000	0.014

Each row describes the potential during a stage of the reversal process. Reversed field is shown in the top row (n = 1) and normal field at the bottom (n = 15).

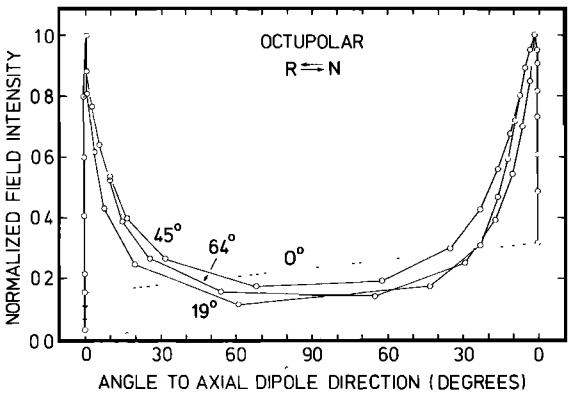

Fig. B3. Normalized field intensity versus angular deviation of field direction for the octupolar zonal flooding model. Curves are drawn for an R-N reversal with equatorial initiation or for an N-R reversal with polar initiation. VGP paths in the northern (southern) hemisphere are near (far) sided. Notice that minimum field intensity is relatively insensitive to site latitude.

octupolar term early in the reversal and of 22% in the quadrupolar term toward the end.

Acknowledgments. We thank Mark Linker and Jack Harter for their valuable assistance during the field work. Thorough reviews of the manuscript by Sherman Grommé, Michel Prévot, Kenneth Hoffman, Joe Rosenbaum, and Charles Denham were all very helpful. This work was supported by grants from the National Science Foundation, Geological Society of America and Sigma Xi.

REFERENCES

Arai, Y., Secular variation in the intensity of the past geomagnetic field, MS thesis, Univ. of Tokyo, Japan, 1963.

Bogue, S. W., Behavior of the geomagnetic field during successive reversals recorded in basalts on Kauai, Hawaii, Ph.D. thesis, Univ. of Calif., Santa Cruz, 1982.

Bogue, S. W., and R. S. Coe, Successive paleomagnetic reversal records from Kauai, *Nature*, *295*, 399–401, 1982.

Clement, B. M., and D. V. Kent, The upper Olduvai polarity transition as recorded in a southern hemisphere deep-sea core (abstract), *Eos Trans. AGU*, *64*, 219, 1983.

Coe, R. S., Paleo-intensities of the earth's magnetic field determined from Tertiary and Quaternary rocks, *J. Geophys. Res.*, *72*, 3247–3262, 1967*a*.

Coe, R. S., The determination of paleo-intensities of the earth's magnetic field with emphasis on mechanisms which could cause non-ideal behavior in the Thellier's method, *J. Geomagn. Geoelectr.*, *19*, 157–179, 1967*b*.

Coe, R. S., C. S. Grommé, and E. A. Mankinen, Geomagnetic paleointensities from radiocarbon-dated lava flows on Hawaii and the question of the Pacific nondipole low, *J. Geophys. Res.*, *83*, 1740–1756, 1978.

Dodson, R., J. R. Dunn, M. Fuller, I. Williams, H. Ito, V. Schmidt, and Y.-M. Wu, Paleomagnetic record of a late Tertiary field reversal, *Geophys. J. R. Astron. Soc.*, *53*, 373–412, 1978.

Doell, R. R., Paleomagnetism of lava flows from Kauai, Hawaii, *J. Geophys. Res.*, *77*, 862–876, 1972.

Doell, R. R., and G. B. Dalrymple, Potassium-argon ages and paleomagnetism of the Waianae and Koolau Volcanic Series, Oahu, Hawaii, *Geol. Soc. Am. Bull.*, *84*, 1217–1242, 1973.

Dunn, J. R., M. Fuller, H. Ito, and V. A. Schmidt, Paleomagnetic study of a reversal of the earth's magnetic field, *Science*, *172*, 840–844, 1971.

Fisher, R. A., Dispersion on a sphere, *Proc. R. Soc. London Ser. A.*, *217*, 295–305, 1953.

Fuller, M., I. Williams, and K. A. Hoffman, Paleomagnetic records of geomagnetic field reversals and the morphology of the transitional fields, *Rev. Geophys. Space Phys.*, *17*, 179–203, 1979.

Hide, R., Self-exciting dynamos and geomagnetic polarity changes, *Nature*, *293*, 728–729, 1981.

Hillhouse, J., and A. Cox, Brunhes-Matuyama polarity transition, *Earth Planet. Sci. Lett.*, *29*, 51–64, 1976.

Hoffman, K. A., Polarity transition records and the geomagnetic dynamo, *Science*, *196*, 1329–1331, 1977.

Hoffman, K. A., Behavior of the geodynamo during reversals: A phenomenological model, *Earth Planet. Sci. Lett.*, *44*, 7–17, 1979.

Hoffman, K. A., Paleomagnetic excursions, aborted reversals and transitional fields, *Nature*, *294*, 67–69, 1981.

Hoffman, K. A., and M. Fuller, Transitional field configurations and geomagnetic reversals, *Nature*, *273*, 715–718, 1978.

Jackson, E. D., E. A. Silver, and G. B. Dalrymple, Hawaiian-Emperor chain and its relation to Cenozoic circumpacific tectonics, *Geol. Soc. Am. Bull.*, *83*, 601–618, 1972.

Kaporovich, I. G., Z. V. Makarova, G. N. Petrova, and R.-S. Rybak, The transitional stage of the geomagnetic field in the Pliocene in the territory of Turkmenia and Azerbaidzhan, *Phys. Solid Earth*, *1*, 59–64, 1966.

Kawai, N., Y. Otofuji, and K. Kobayashi, Paleomagnetic study of deep-sea sediments using thin-sections, *J. Geomagn. Geoelectr.*, *28*, 395–412, 1976.

Liddicoat, J. C., Gauss-Matuyama polarity transition, *Phil. Trans. R. Soc. London Ser. A*, *A306*, 121–128, 1982.

Macdonald, G. A., D. A. Davis, and D. C. Cox, Geology and groundwater resources of the island of Kauai, Hawaii, *Bull. Hawaii Div. Hydrogr.* 13, 1960.

Mankinen E. A., J. M. Donnely-Nolan, C. S. Grommé, and B. C. Hearn Jr., Paleomagnetism of the Clear Lake volcanics and new limits on the age of the Jaramillo normal polarity event, in Research in the Geysers-Clear Lake geothermal area, northern California, *U.S. Geol. Surv. Prof. Pap.*, *1141*, 67–82, 1981.

McDougall, I., Age of shield-building volcanism of Kauai and linear migration of volcanism in the Hawaiian Island chain, *Earth Planet. Sci. Lett.*, *46*, 31–42, 1979.

McFadden, P. L., and M. W. McElhinny, Variations in the geomagnetic dipole, *2*, Statistical analysis of VDMs for the past 5 million years, *J. Geomagn. Geoelectr.*, *34*, 163–189, 1982.

Opdyke, N. D., D. V. Kent, and W. Lowrie, Details of magnetic polarity transitions recorded in a high deposition rate deep-sea core, *Earth Planet. Sci. Lett.*, *20*, 315–324, 1973.

Petrova, G. N., V. V. Bukha, L. N. Gamov, G. Z. Gurariy, V. F. Davydov, T. A. Ismail-Zade, Yu. D. Kalinin, A. Ya. Kravchinskiy, G. A. Pospelova, and V. P. Rodinov, Characteristic features of transient regimes of the geomagnetic field, *Phys. Solid Earth*, *6*, 369–384, 1972.

Prévot, M., E. A. Mankinen, S. Grommé, and A. Lecaille, High paleointensities of the geomagnetic field from thermomagnetic studies on rift-valley pillow basalts from the Mid-Atlantic ridge, *J. Geophys. Res.*, *88*, 2316–2326, 1983.

Shaw, J., A new method for determining the magnitude of the paleomagnetic field: Application to five historic flows and five archaeological samples, *Geophys. J. R. Astron. Soc.*, *12*, 239–258, 1974.

Shaw, J., Strong geomagnetic fields during a single Icelandic polarity transition, *Geophys. J. R. Astron. Soc.*, *40*, 345–350, 1975.

Tarling, D. H., The paleomagnetism of some of the Hawaiian Islands, *Geophys. J. R. Astron. Soc.*, *10*, 93–104, 1965.

Thellier, E., and O. Thellier, Sur l'intensitié du champ magnétique terrestre dans le passé historique et géologique, *Ann. Geophys.*, *15*, 285–376, 1959.

Turner, D. L., R. D. Jarrard, and R. B. Forbes, Geochronology and origin of the Prett-Walker seamount chain, Gulf of Alaska: A new pole of rotation for the Pacific plate, *J. Geophys. Res.*, *85*, 6547–6556, 1980.

Valet, J.-P., and C. J. Laj, Paleomagnetic record of two successive Miocene geomagnetic reversals in western Crete, *Earth Planet. Sci. Lett.*, *54*, 53–63, 1981.

Van Zijl, J. S. V., K. W. T. Graham, and A. L. Hales, The paleomagnetism of the Stormberg lavas of South Africa, 2, The behavior of the magnetic field during a reversal, *Geophys. J. R. Astron. Soc.*, *7*, 169–182, 1962.

Watkins, N. D., Non-dipole behaviour during an upper Miocene geomagnetic polarity transition in Oregon, *Geophys. J. R. Astron. Soc.*, *17*, 121–149, 1969.

Williams, I., and M. Fuller, Zonal harmonic models of reversal transition fields, *J. Geophys. Res.*, *86*, 11657–11665, 1981.

Williams, I., and M. Fuller, A Miocene polarity transition (R-N) from the Agno Batholith, Luzon, *J. Geophys. Res.*, *87*, 9408–9418, 1982.

S. W. Bogue, Department of Geological Sciences, AJ-20, University of Washington, Seattle, WA 98195.

R. S. Coe, Earth Sciences Board, University of California, Santa Cruz, CA 95064.

(Received April 21, 1983;
revised February 16, 1984;
accepted May 29, 1984.)